**Please cite the Published Version**

**Additional Information:** This is an open access article published in Journal of Environmental Chemical Engineering, by Elsevier.

**Data Access Statement:** Data will be made available on request.

# Sustainable silver nanoparticle-enhanced additive manufactured sensor for cadmium (II) sensing in environmental waters

Karen K.L. Augusto [a,b,1], Elena Bernalte [a,*,1], Robert D. Crapnell [a], Hayley G. Andrews [a], Orlando Fatibello-Filho [b,c], Craig E. Banks [a,*]

[a] *Faculty of Science and Engineering, Manchester Metropolitan University, Dalton Building, Chester Street, M1 5GD, Great Britian*
[b] *Laboratório de Analítica, Bioanalítica, Biosensores, Electroanalítica e Sensores, Departamento de Química, Universidade Federal de São Carlos (UFSCar), CP 676, São Carlos, SP 13560-970, Brazil*
[c] *National Institute of Science and Technology of Nanomaterials for Life (INTC Nano Vida), Brazil*

A B S T R A C T

The development of bespoke, high-performance conductive filament is critical to address limitations of current additively manufactured sensors. In particular, enhancing the sensitivity and reliability of this technology is vital toward their in-the-field applications such as water pollution monitoring. As such, we present the production of filament containing a mix of carbon black (CB) and graphite (G) functionalised with silver nanoparticles (AgNPs) that does not require special printing conditions, special instrumentation, or any post-print modification for the detection of cadmium (II) in environmental waters. The AgNPs are synthesised on graphite flakes using an eco-friendly, aqueous synthesis, without additional reducing agents and their presence is confirmed through SEM, EDX and XPS analysis. The AgNP loaded graphite is incorporated into a filament using recycled PLA and the bio-based plasticiser castor oil, ensuring sustainability is at the heart of the work. The electrodes produced a heterogeneous rate constant, $k^0$, of $(1.9 \pm 0.2) \times 10^{-3}$ cm s$^{-1}$ and were applied toward the detection of cadmium (II) within buffer, tap water, and river water samples. Importantly, using electrodes straight from the print bed with no post-print modification, a Limit of Detection of 0.43 µg L$^{-1}$ and a Limit of Quantification of 1.44 µg L$^{-1}$ towards the sensing of cadmium (II), significantly below the worldwide targets of 3–5 µg L$^{-1}$, was achievedwas achieved. This work shows a simple but effective approach to include metallic nanoparticles within conductive additive manufacturing filament and the capabilities towards monitoring heavy metal contaminants in water systems.

## 1. Introduction

Heavy metals are considered significant pollutants in the environment due to their use within industry and subsequent discharge into the environment. Cadmium (II) is one such metal, although found naturally at low concentrations ($<1$ µg L$^{-1}$) in unpolluted environmental water, anthropogenic activity such as mining, zinc refining, plastic manufacturing and the use of fertilizers have contributed to rising levels [1]. Exposure to cadmium, in addition to other toxic heavy metals, is an issue due to their ability to bind with protein sites, displacing the essential metals, bio-accumulating and eventually harming the body [2]. Through this, cadmium can induce serious health risks such as cancer, renal dysfunction, hypertension, and immune/nervous system damage [3]. As such, the World Health Organisation (WHO) have placed a maximum permissible level of 3 µg L$^{-1}$ in drinking water [4] and therefore regular monitoring and the ability to quantify the levels of cadmium (II) is vital. The detection of these pollutants within water sources is an important part of alignment with the United Nations (UN) Sustainable Development Goals (SDGs), in particular Goal 6 entitled "Clean Water and Sanitation", which states that safe drinking water is out of reach for billions of people around the world.

Due to the importance of detecting cadmium (II), numerous methodologies have been extensively reported within the literature. These include inductively coupled plasma-mass spectrometry (ICP-MS) [5], inductively coupled plasma-optical emission spectrometry (ICP-OES) [6], atomic absorption spectroscopy [7], and atomic fluorescence

spectroscopy [8]. Although these methods offer excellent analytical performance, they are costly, limited to being based within a laboratory, requiring a skilled user, and meticulous transport and preservation of the samples. On the other hand, electrochemistry offers a viable route to overcome these issues with the additional advantage of feasibility for on-site screening of water samples. Along with the revolution experience in the last decade involving the development of robust and reliable portable instrumentation, electroanalysis has transformed into a simple, more user-friendly and low-cost methodology that can be performed in-situ, meaning that it can be used anywhere in the world [9]. Various electroanalytical methodologies have been reported for the detection of cadmium (II), with the main focus on modifying the electrode material [3]. Classical electrodes, such as a glassy carbon or boron-doped diamond, are very costly and require significant treatment between runs making them inefficient for this application. The rise of screen-printed electrodes have offered a route toward single-use sensors that have significant scales of efficiency [10], however the use of plastic substrates and organic solvents in the production is an obvious concern for environmental reasons. Additionally, although cheap to make, the equipment required for reliable screen-printing would require significant investment and a set location. In this regard, additive manufacturing electrochemistry becomes an attractive technique.

Fused filament fabrication (FFF), also referred to as Fused Deposition Modelling (FDM), is the most utilised additive manufacturing technique within electrochemistry. It has been employed in the production of electrochemical equipment, accessories, and notably electrodes [11–13]. FFF operates by depositing thermoplastic filament in a layer-by-layer fashion building the 3D object as specified within the design. FFF offers significant advantages over traditional manufacturing techniques such as the low cost of equipment and materials, the ability for on-demand manufacturing, very low waste production, short lead times, a high degree of customisability, and ease of global collaboration [14]. These advantages have seen additive manufacturing gain significant interest in many fields of industry and academia, but the availability of electrically conductive commercial filament has been a key factor driving the growth of additive manufacturing within electrochemistry. Initially, there were significant publications on how to "activate" the electrodes printed from these commercial materials to try to remove surface polymer and improve their electrochemical performance [15–18], as well as optimising printing and design parameters [19–23]. Through these methods some interesting sensor designs were produced [13,24–26] including for cadmium (II) [27,28]; however, the poor conductivity of the filament used inhibits the ability for these platforms to challenge traditional electrodes and the necessity to activate electrodes is a huge block toward commercialisation. As such, researchers have begun to produce their own bespoke filaments designed for their specific applications.

The production of bespoke conductive filament has been summarised in the literature [29], where various filaments have been produced that significantly improve on the conductivities provided by the commercial alternative. Initially, these began as carbon black (CB) loaded filaments within poly(lactic acid) (PLA) for use within energy storage [30] and electroanalysis [31]. Since then, researchers have further improved the characteristics of filament through using mixed carbon materials [32–35] to either improve the conductivity or reduce the material cost of production. Additionally, there are reports of alternative base polymers to improve the chemical stability [36,37], and a drive for improved sustainability through using recycled polymers [31–36,38,39], replacing CB with graphite [34,35], or through using bio-based plasticisers [39]. Recently, acknowledging the importance of advancing with this technology for electroanalytical applications, Koukouviti et al. [40] have reported the inclusion of the base metals copper and bismuth for the production of specialised filament, however there has been no reports of precious metal embedded filament. To further progress the field of additive manufacturing electrochemistry and create bespoke filament of exceptional electrochemical properties, the inclusion of precious

metal nanoparticles is desired. The interest in the use of silver nanoparticles (AgNPs) in electroanalytical applications is enormous as their catalytic properties result in an improvement of the sensing performance of the electrodes [41]. Some methods employed in the literature to modify electrodes with silver nanoparticles are included in the Table S1. Electrodeposition and solution drop-casting are the most applied, which are often complicating electrode modifications due to reproducibility problems at large scale [42] and limited conductivity of commercial filaments [43]. In this work, we propose a new method that facilitates integrating AgNPs synthesis to the additive manufacturing methodologies for the fabrication of highly conductive polymers that will help realise scenarios where most-common post-print modifications of electrodes are not required.

Therefore, we look to synthesise silver nanoparticles (AgNPs) onto graphite using an eco-friendly methodology modified from work by Pandey et al. [44]. Such modified graphite containing AgNPs is used to directly produce high performance conductive PLA filament applied for the electroanalytical detection of cadmium ($Cd^{2+}$) in environmental waters without further modifications. This approach will overcome current obstacles for the commercial viability of additive manufacturing electrochemistry and encourage a step change in how in situ environmental monitoring can be achieved.

## 2. Experimental section

### 2.1. Chemicals

All chemicals used throughout this work were used as received without any further purification. All aqueous solutions were prepared with deionised water of a measured electric resistivity not less than 18.2 MΩ cm, sourced from a Milli-Q Integral 3 system from Millipore UK (Watford, UK). Hexaammineruthenium (III) chloride (98 %), castor oil, potassium ferricyanide (99 %), potassium ferrocyanide (98.5–102 %), sodium hydroxide (>98 %), potassium chloride (99.0–100.5 %), graphite powder (<20 μm), boric acid (≥99.5 %), phosphoric acid (≥85 %), acetic acid (≥99 %), nitric acid (70 %) and cadmium standard for AAS were purchased from Merck (Gillingham, UK). Silver nitrate (>99 %) was purchased from Alfa Aesar (Massachusetts, USA). Carbon black was purchased from PI-KEM (Tamworth, UK). Recycled poly(lactic acid) (rPLA) was purchased from Gianeco (Turin, Italy). River water samples were obtained in accordance with EPA guidelines from the River Irwell, Greater Manchester, UK (approx. location: 53.517464, −2.302739). Tap water samples were obtained from laboratory 5.39, John Dalton Tower, Manchester, UK.

### 2.2. Silver nanoparticles (AgNPs) synthesis on graphite

The AgNPs were synthesised directly onto graphite flakes based on the procedure reported by Pandey et al. [44] performed on graphite sheet. Briefly, a 50 mL solution of AgNO$_3$ (20 mg mL$^{-1}$) was prepared, to which 20 g of graphite powder was added. This was placed on a stirrer plate at room temperature and left to stir overnight, after which the solution was removed through vacuum filtration on a standard filter paper and dried in the oven at 60 °C. This powder was then ready for use within filament production.

### 2.3. Recycled filament production

Recycled polylactic acid (rPLA) was dried in an oven at 60 °C for a minimum of 2.5 h before use to remove any residual water in the polymer. The polymer composition was achieved through the addition of appropriate amounts of rPLA, castor oil, carbon black (CB), and functionalised graphite in a chamber of 63 cm$^3$. All filaments made throughout this work utilised 10 wt% castor oil as a plasticiser [39], the amount of PLA, CB and graphite were used as previously tested [45]. The compounds were mixed using a Thermo Haake Polydrive dynameter

fitted with a Thermo Haake Rheomix 600 (Thermo-Haake, Germany) at 190 °C with Banbury rotors at 70 rpm for 5 min. The resulting polymer composites were allowed to cool to room temperature before being granulated to create a finer particle size using a Rapid Granulator 1528 (Rapid, Sweden). The polymer composites were collected and processed through the hopper of a EX2 extrusion line (Filabot, VA, United States). The EX2 was set up with a single screw with two set heat zones of 60, and 195 °C, respectively. The molten polymer was extruded from a 1.75 mm die head, pulled along an airpath cooling line (Filabot, VA, United States) and collected on a spool. After which, the filament was then ready to use for additive manufacturing.

### 2.4. Additive manufacturing of the electrodes

All computer designs and 3MF files in this manuscript were produced using Fusion 360® (Autodesk®, CA, United States). These files were sliced and converted to GCODE files in PrusaSlicer (Prusa Research, Prague, Czech Republic). The additive manufactured electrodes were produced using fused filament fabrication (FFF) technology on a Prusa i3 MK3S+ (Prusa Research, Prague, Czech Republic). All additive manufactured electrodes were printed using identical printing parameters, namely a 0.6 mm nozzle with a nozzle temperature of 215 °C, 100 % rectilinear infill [19], 0.15 mm layer height, and print speed of 35 mm s$^{-1}$.

### 2.5. Physicochemical characterisation

X-ray Photoelectron Spectroscopy (XPS) data were acquired using an AXIS Supra (Kratos, UK), equipped with a monochromatic Al X-ray source (1486.6 eV) operating at 225 W and a hemispherical sector analyser. It was operated in fixed transmission mode with a pass energy of 160 eV for survey scans and 20 eV for region scans with the collimator operating in slot mode for an analysis area of approximately $700 \times 300$ μm, the FWHM of the Ag 3d5/2 peak using a pass energy of 20 eV was 0.613 eV. The binding energy scale was calibrated by setting the graphitic sp$^2$ C 1 s peak to 284.5 eV; this calibration is acknowledged to be flawed [46] but was nonetheless used in the absence of reasonable alternatives, and because only limited information was to be inferred from absolute peak positions.

Scanning Electron Microscopy (SEM) micrographs were obtained using a Crossbeam 350 Focussed Ion Beam – Scanning Electron Microscope (FIB-SEM) (Carl Zeiss Ltd., Cambridge, UK) fitted with a field emission electron gun. Secondary electron imaging was completed using a Secondary Electron Secondary Ion (SESI) detector. Energy Dispersive X-ray Spectroscopy (EDX) analysis was performed using an Ultim Max 170 detector (Oxford Instruments plc, Abingdon, UK.) installed on the FIB-SEM. An acceleration voltage of 20 kV was used to image the samples for EDX analysis experiments. Samples were mounted on the aluminium SEM pin stubs (12 mm diameter, Agar Scientific, Essex, UK) using adhesive carbon tabs (12 mm diameter, Agar Scientific, Essex, UK) and coated with a 5 nm layer of Au/Pd metal using a Leica EM ACE200 coating system before imaging. Quantification of EDX spectra was carried out using a standardless quantification procedure developed by Oxford Instruments and integrated into the AZtec 6.1 (Oxford Instruments, Abingdon, UK).

X-ray diffraction (XRD) measurements were performed on the powder graphite samples to obtain the structural information using PANalytical X'Pert Powder X-ray diffractometer with Cu (λ = 1.54 Å) as the source with 45 kV voltage and 40 mA current settings. The data were collected in a continuous mode over the 2Ө scan range of 5° – 90°, with a step size of 0.01° for 108 seconds per step at room temperature under ambient conditions. The samples were spinning at 16 rpm during the measurements for uniform data collection. PreFIX module on the incident beam side with the automatic divergence and fixed anti-scatter slit of 4° along with PreFIX module on the diffracted side with PIXcel 1D detector in scanning line mode with programmable anti-scatter slit were used to collect the diffraction patterns from a constant irradiated length of 0.5 mm.

### 2.6. Electrochemical experiments

All electrochemical experiments were performed on an Autolab 100 N potentiostat controlled by NOVA 2.1.7 (Utrecht, The Netherlands). Identical additive manufactured electrodes were used throughout this work for all filaments, printed in a lollipop shape (Ø 5 mm disc with 8 mm connection length and $2 \times 1$ mm thickness [20]) alongside an external commercial Ag|AgCl/KCl (3 M) reference electrode with a nichrome wire counter electrode. Note that the electrode is connected using a crocodile clip where only the circular part is carefully immersed in the solution to perform the experiments. All solutions of $[Ru(NH_3)_6]^{3+}$ were purged of $O_2$ thoroughly using $N_2$ prior to any electrochemical experiments. Solutions of $[Fe(CN)_6]^{4-}$ were prepared in the same way without the need of further degassing. Note that electrochemical cells and additional glassware used in this work has been pre-treated accordingly for trace heavy metals analysis prior to use, which involved a 24 h immersion in 10 % nitric acid solution, rinse with deionised water and keep in sealed bags to avoid further contamination.

Electrochemical impedance spectroscopy (EIS) was recorded in the frequency range 0.1 Hz to 100 kHz applying 10 mV of signal amplitude to perturb the system under quiescent conditions. NOVA 2.1.7 software was used to fit Nyquist plots obtained to adequate equivalent circuit.

Activation of the additive manufactured electrodes was performed before the electrochemical experiments using $[Fe(CN)_6]^{4-}$. This was achieved electrochemically in 0.5 M NaOH, as described in the literature [47]. Briefly, the additive manufactured electrodes (CB/Ag-G/PLA) were connected as the working electrode in conjunction with a nichrome wire coil counter and Ag|AgCl/KCl (3 M) reference electrode and placed in a solution of 0.5 M NaOH. Chronoamperometry was used to activate the additive manufactured electrodes by applying a set voltage of + 1.4 V for 200 s, followed by applying -1.0 V for 200 s. The additive manufactured electrodes were then thoroughly rinsed with deionised water and dried under compressed air before further use.

## 3. Results and discussion

### 3.1. Synthesis of silver nanoparticles (AgNPs) on graphite and incorporation into filament

AgNPs were produced on the surface of graphite flakes utilising an eco-friendly methodology, Fig. 1 A, involving the submersion of graphite powder within a 20 mg mL$^{-1}$ aqueous solution of AgNO$_3$ with stirring overnight. This methodology didn't utilise any solvents other than water, as well as no addition of reducing agents, instead relying solely on the reducing nature of graphite. Once filtered and dried, the modified graphite powder was characterised to identify the presence of AgNPs. Fig. 1B shows a micrograph obtained for the modified graphite, where the presence of small spherical moieties can be seen predominantly on the edges of the graphite flakes.

To further confirm the presence of silver on the graphite surface, EDX mapping was performed on selected areas. An example region, along with its corresponding carbon and silver maps, is shown in Fig. 1 C, 1D, and 1E, respectively. These maps reveal that the majority of the composition consists of carbon, corresponding to the graphite flakes, while small, dispersed silver particles appear as distinct spherical points across the sample.

XRD analysis was then performed on graphite powder modified with AgNPs, Fig. 1 F. The XRD pattern of AgNP-graphite shows several reflection peaks at 2Ө values of 37.84°, 44.37°, 54.33° and 77.34°, which correspond to the (111), (200), (142) and (311) planes of the face-centred cubic (fcc) crystal structure of silver (JCPDS, No. 04–0783), confirming the crystalline nature of the AgNPs formed on the surface of graphite [48,49]. Furthermore, the crystallite sizes were determined
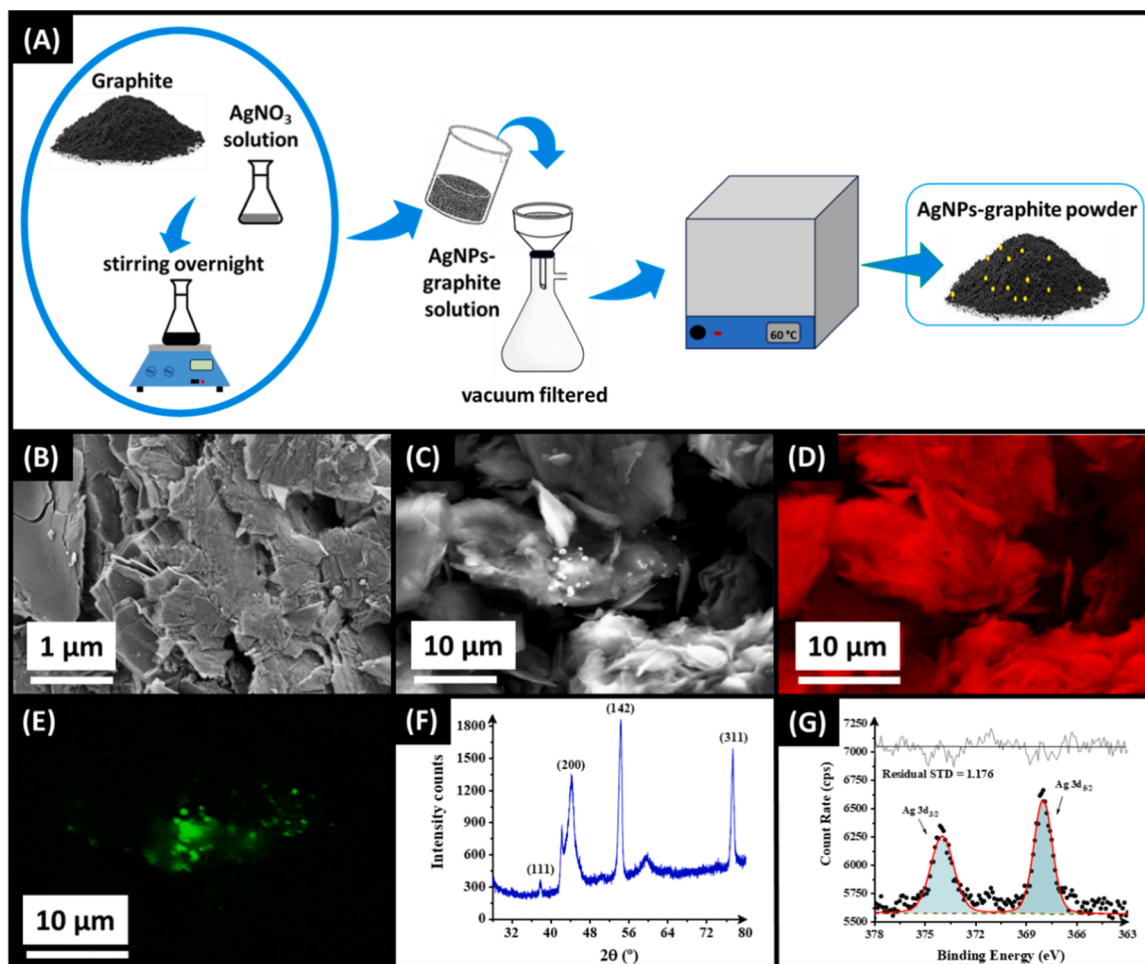
**Fig. 1.** (A) Schematic representation of AgNP-graphite production. (B) SEM image for modified graphite powder. (C to E) EDX elemental mapping analysis of graphite area, carbon map, and silver map, respectively. (F) XRD pattern of AgNP-graphite and (G) XPS data for AgNP-graphite.

from the reflection peaks for AgNPs using the Debye-Scherrer Eq. (1) [50,51]:

$$D = k \lambda / (\beta \cos \theta) \tag{1}$$

Where D represents the average crystallite size calculated for all the reflection peaks, k is the Scherrer constant commonly taken as 0.94 [52], $\lambda$ is the wavelength of X-ray source, $\beta$ is the corrected sample peak broadening or full width at half maximum (FWHM) and $\theta$ is the Bragg diffraction angle at peak position.

Considering the four identified peaks, the average size of AgNPs deposited on graphite using the described sustainable approach was $15.05 \pm 4.07$ nm, confirming the nano-size nature of the likely AgNPs synthesised.

To further confirm the presence of the AgNPs on the surface of the graphite, the samples were analysed through XPS. Fig. 1 G reveals two main peaks at 368 eV and 374 eV, corresponding to Ag $3d_{5/2}$ and Ag $3d_{3/2}$, respectively. The fitting of these peaks yields an RSD of 1.176. These results align with previous reports in the literature [53,54], confirming the presence of Ag on the surface of the graphite. Once the presence of AgNP on the graphite was confirmed this was incorporated into conductive additive manufacturing filament. To create high performance conductive filament with graphite, it is important to use a combination of carbon black and graphite [34,35]. Using a total carbon loading of 30 wt%, with the optimised ratio of CB (18 %) to graphite (12 %) established previously [35], filaments were produced incorporating AgNP-modified graphite (CB/Ag-G/PLA). The impressive low-temperature flexibility of the produced filament is presented in

Figure S1A, which is attributed to the castor oil plasticiser [39]. In addition to flexibility, the filament showed excellent conductivity with bulk resistance across 10 cm of filament measured to be $(422 \pm 33)$ $\Omega$ for the CB/Ag-G/PLA. Once the filament was available, additively manufactured electrodes were produced ready for electrochemical characterisation. Figure S1B shows the high quality print definition of lollipop electrode accomplished with the CB/Ag-G/PLA filament.

### 3.2. Electrochemical characterisation of the additive manufactured electrodes

The additively manufactured electrodes printed from the AgNP filament were electrochemically characterised against both the near-ideal outer-sphere redox probe hexaamineruthenium (III) chloride [Ru $(NH_3)_6]^{3+}$ (1 mM in 0.1 M KCl) and the commonly used inner-sphere probe [Fe(CN)$_6$]$^{4-}$ (1 mM in 0.1 M KCl). Initially, potential scan rate studies (5–500 mV s$^{-1}$) were performed against [Ru(NH$_3$)$_6$]$^{3+}$ (1 mM in 0.1 M KCl) as this allowed for the best determination of the heterogeneous electron (charge) transfer rate constant ($k^0$) and the real electrochemical surface area ($A_e$) [55]. An example of the potential scan rate obtained additively manufactured electrodes printed from the only-graphite filament and the AgNP filament are presented in Figs. 2A and 2B. In both cases, the appropriate redox couple for [Ru(NH$_3$)$_6$]$^{3+}$ (1 mM in 0.1 M KCl) is observed with a one-electron reduction peak observed at ~-0.2 V with a defined and crisper wave shape. The inset in Figs. 2A and 2B are the corresponding Randles- Ševčík plot confirming the diffusion-controlled nature of the electrochemical processes. The
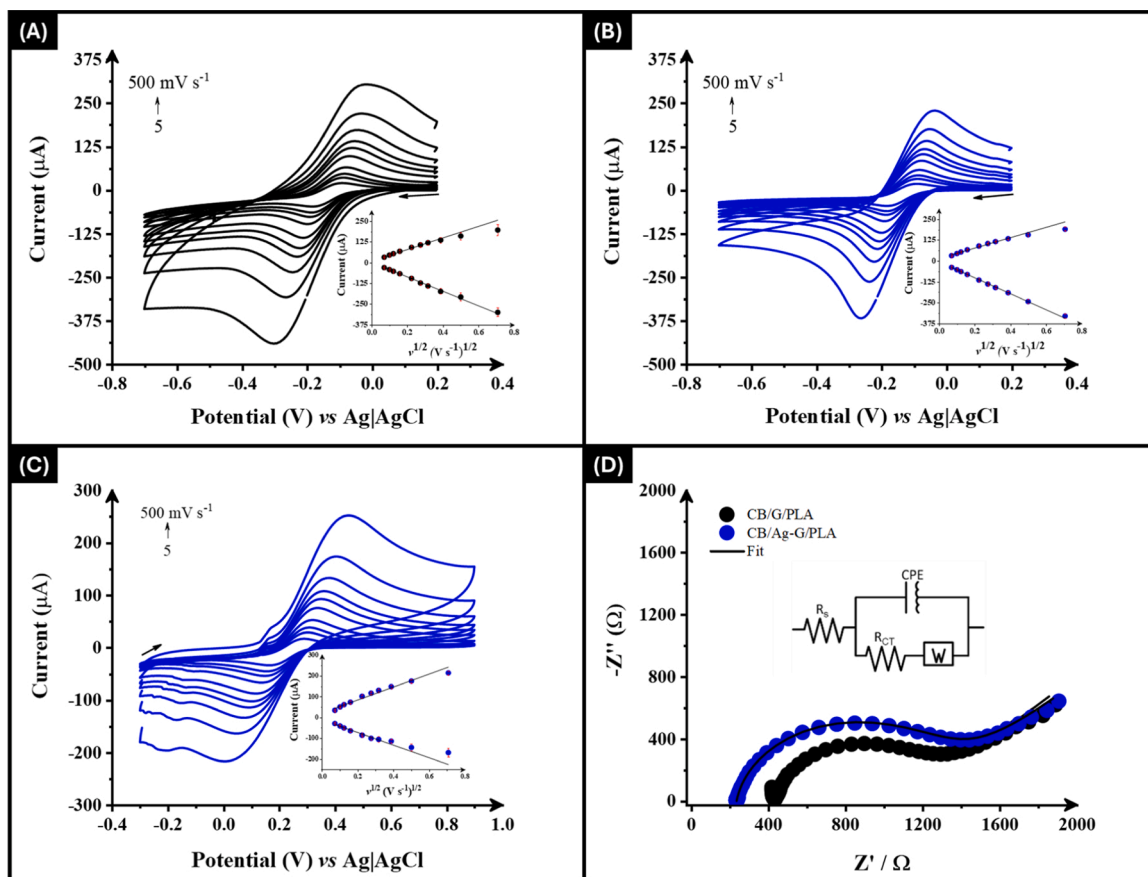
**Fig. 2.** Potential scan rate study (5–500 mV s$^{-1}$) with $[Ru(NH_3)_6]^{3+}$ (1 mM in 0.1 M KCl) performed in the (A) only-graphite (CB/G/PLA) and (B) AgNP-graphite (CB/Ag-G/PLA) as the WE, respectively. Inset: Randles–Ševčík plot. (C) Potential scan rate study (5–500 mV s$^{-1}$) with $[Fe(CN)_6]^{4-}$ (1 mM in 0.1 M KCl) performed in the AgNP-graphite as the WE. Inset: the Randles–Ševčík plot. (D) Comparison of EIS Nyquist plots of $[Fe(CN)_6]^{4-/3-}$ using only graphite (CB/G/PLA) and AgNP-graphite (CB/Ag-G/PLA) electrodes. Inset: the proposed equivalent circuit.

calculated $k^0$ for the only-graphite electrode was $(1.75 \pm 0.06) \times 10^{-3}$ cm s$^{-1}$ compared to AgNP-graphite electrodes where it was $(1.93 \pm 0.015) \times 10^{-3}$ cm s$^{-1}$, with a corresponding real electrochemical surface area of $(0.53 \pm 0.03)$ cm$^2$ and $(0.62 \pm 0.03)$ cm$^2$ for only-graphite and AgNP-graphite electrodes, respectively. Additionally, cyclic voltammetry at 50 mV s$^{-1}$ revealed a peak-to-peak separation of $(0.124 \pm 0.003)$ V and $(0.118 \pm 0.008)$ V for only-graphite and AgNPs-graphite electrodes, highlighting the favourable electron transfer characteristics attributed to the presence of AgNP.

The electrodes were then further tested against the commonly used inner-sphere probe $[Fe(CN)_6]^{4-/3-}$ (1 mM in 0.1 M KCl) as this molecule cannot react electrochemically via quantum electron tunnelling [56]. The potential scan rate study (5–500 mV s$^{-1}$) for $[Fe(CN)_6]^{4-}$(1 mM in 0.1 M KCl) using the AgNP electrode is presented in Fig. 2C, with the Randles- Ševčík equation once again inset showing the electrochemical process is of a diffusion-controlled nature. Finally, the AgNP electrodes were compared with the graphite-only electrodes using electrochemical impedance spectroscopy (EIS) in a $[Fe(CN)_6]^{4-/3-}$ solution (1 mM in 0.1 M KCl), with the corresponding Nyquist plot shown in Fig. 2D. From this plot, both the solution resistance ($R_S$) and charge-transfer resistance ($R_{CT}$) of the electrodes were determined through circuit fitting, with the applied circuit shown as an inset in Fig. 2D. The results suggest no substantial improvement in charge-transfer resistance, given the variations in standard deviation. The $R_{CT}$ values were 0.91 ($\pm 0.27$) k$\Omega$ for CB/G/PLA and 1.08 ($\pm 0.10$) k$\Omega$ for CB/Ag-G/PLA. However, a notable improvement in solution resistance was observed for the CB/Ag-G/PLA electrode. The $R_S$ value for CB/Ag-G/PLA was 236 ($\pm 5$) $\Omega$, significantly lower than the 432 ($\pm 4$) $\Omega$ measured for CB/G/PLA, indicating reduced

resistance introduced by the CB/Ag-G/PLA electrode. Having electrochemically characterised the AgNP electrodes, we now move toward testing them toward the electroanalytical determination of cadmium (II).

### 3.3. Electroanalytical determination of cadmium (II)

The detection of cadmium (II) within water samples is important to meet the United Nations Sustainable Development Goals 6 entitled Clean Water and Sanitation. Cadmium accumulates in the body, within the kidneys, whereby the associated renal tubular damage is linked to the impaired reabsorption of proteins, glucose and amino acids. Governing bodies across the board have set exposure limits for cadmium of 5 µg L$^{-1}$, including the United States Environmental Protection Agency (EPA) and the European Union (EU). As such, 5 µg L$^{-1}$ is the minimum requirement for the development of new sensors in this field. To achieve this level of sensitivity it is common within electroanalysis to look toward pulse techniques and therefore we look to explore both differential pulse voltammetry (DPV) and square-wave voltammetry (SWV) to this end. Additionally, for additively manufactured electrodes to be easily commercialised the removal of activation procedures is necessary and as such all the electrodes used for electroanalysis will be used without any post print treatment. The electrochemical mechanism involved in the detection of cadmium (II) on CB/Ag-G/PLA is described as:

$$Cd^{2+}(aq) + 2e^-(m) \rightarrow Cd^0(s) \qquad (2)$$

To test the CB/Ag-G/PLA electrodes towards the detection of cadmium (II) we first optimised the buffer for the laboratory measurements,

Figure S2. Britton Robinson (BR) buffer (pH = 5.0) and BR buffer (pH = 5.0) with 0.1 M KCl were tested for the detection of 100 µg L$^{-1}$, where it was found that the addition of KCl did not improve the performance of the system. Following this, the deposition potentials (Figure S3) and deposition times (Figure S4) were optimised for both the DPV and SWV techniques. It was concluded that a deposition potential of −1.0 V and time of 60 s was optimal for DPV, and a potential of −1.1 V and time of 60 s was optimal for SWV. Finally, the parameters for both DPV and SWV were optimised, with the final values found in Table S2.

Using these optimised settings, CB/G/PLA and CB/Ag-G/PLA electrodes were tested for the detection of 100 µg L$^{-1}$ cadmium (II) with the SWV results shown in Fig. 3 A. It can be seen clearly in both cases that the AgNP produces a significantly higher peak current compared to the graphite only electrode, which is attributed to the increased surface area and improved electrochemical performance of the electrode with. To further test the electrode, both the as-printed only graphite and AgNP-graphite electrodes were then used to produce an analytical curve for the detection of cadmium (II) within BR buffer (pH = 5.0) using SWV. The SWV results for the CB/G/PLA and CB/Ag-G/PLA electrodes are overlayed in Fig. 3B for comparative purposes, showing the significant improvement in sensitivity with the electrode containing AgNP graphite. The detection of cadmium (II) using the AgNP electrode was achieved over two linear ranges, between 1.5 – 15 µg L$^{-1}$ and 30 – 100 µg L$^{-1}$. Using this data, the limit of detection (LOD) and limit of quantification (LOQ) could be calculated using 3 times and 10 times the deviation of the blank divided by the gradient of the analytical calibration curve. The LOD for the AgNP electrode was calculated as 0.43 µg L$^{-1}$ and the LOQ at 1.44 µg L$^{-1}$, which are clearly well below the guidelines of 3–5 µg L$^{-1}$ set out by governing bodies. Importantly, this was achieved without activation of the electrode or any other post print modifications, giving enhanced viability toward commercialisation. The repeatability for CB/Ag-G/PLA electrode using both DPV and SWV was then studied, Figure S5. For both techniques the AgNP electrodes produced a 3.06 % deviation using SWV and 5.13 % using DPV, showing excellent reproducibility of this additive manufactured AgNP electrode.

Additionally, possible interferents were tested for both CB/Ag-G/PLA and CB/G/PLA electrodes (Figure S6). The anodic current responses were evaluated in the presence of Pb$^{2+}$, Hg$^{2+}$, and As$^{3+}$ at a 1:1 analyte-to-interferent ratio. When using CB/G/PLA electrodes, the Cd peak current exhibited a substantial increase of 890 % in the presence of Hg$^{2+}$. In contrast, while the CB/Ag-G/PLA electrode also showed a notable increase (284 %), it demonstrated greater resistance to interference compared to CB/G/PLA. Overall, neither Pb$^{2+}$ nor As$^{3+}$ caused significant interference in either electrode. However, the CB/Ag-G/PLA electrode exhibited slightly lower standard deviations in peak currents, indicating better stability in the presence of interfering species.

Finally, having established that SWV was the best technique in combination with the AgNP electrodes, this system was applied to the detection of cadmium (II) within real tap and river water samples. The plot for the AgNP electrode in tap water is shown in Fig. 4A, where a linear range was again found, with a R$^2$ value of 0.98, a LOD of 0.05 µg L$^{-1}$, a LOQ of 0.15 µg L$^{-1}$, and a recovery of 98 %. Within river water, Fig. 4B, once again a linear relationship was found giving an R$^2$ value of 0.99, a LOD of 0.55 µg L$^{-1}$, a LOQ of 1.85 µg L$^{-1}$, and a recovery of 87 %. To further test the system within river water, spiked samples were tested using both the graphite and AgNP electrodes, with the results summarised in Table 1.

This shows that the electrodes printed from the CB/Ag-G/PLA filament can provide excellent sensitivity and accuracy for the detection of cadmium in real environmental water samples. Table S3 shows a comparison between this system and others reported in the literature where the additively manufactured electrode from AgNP filament performs excellently.

## 4. Conclusions

Within this work, we report the production of a novel conductive additive manufacturing filament containing AgNPs (CB/Ag-G/PLA). The AgNPs were synthesised using an eco-friendly methodology where graphite flakes acted as the reducing agent. The AgNP loaded graphite flakes were then incorporated into additive manufacturing filament. The electrodes printed from this filament were electrochemically characterised. The AgNP graphite electrodes produced an k$^0$ value of (1.9 ± 0.2) × 10$^{-3}$ cm s$^{-1}$, showing an excellent electrochemical performance due to the presence of the AgNPs. The electrodes were then applied toward the detection of cadmium (II). Using an optimised SWV methodology, the AgNP electrodes achieved a LOD of 0.43 µg L$^{-1}$ and a LOQ of 1.44 µg L$^{-1}$ which is well below the target of 3–5 µg L$^{-1}$ set by worldwide agencies for the appropriate levels of cadmium in water. The electrodes were successfully used to determine the cadmium (II) concentration within tap and river water samples with recoveries achieved between 87 % and 102 %. These electrodes achieved these impressive levels of sensitivities with no post print-modification or activation procedure which is common within additive manufacturing electrochemistry. This work shows how to include metallic nanoparticles within conductive additive manufacturing filament and the improved electrochemical performance you can achieve through this. With no further requirement for special printers or complex electrode modification, we expect this to motivate researchers to explore electrode materials never
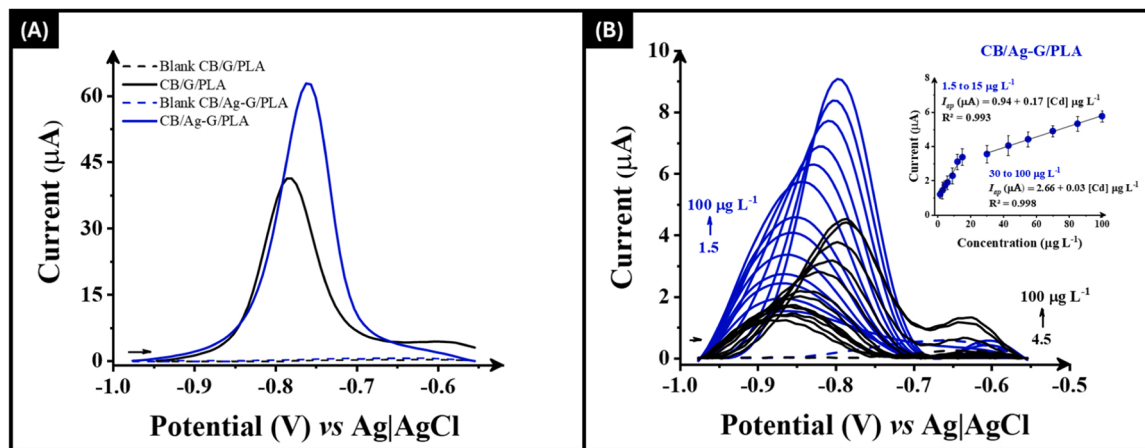


**Fig. 3.** (A) SW voltammograms in the presence of 100 µg L$^{-1}$ of cadmium (II) performed at graphite and AgNP-graphite electrodes in 0.1 mol L$^{-1}$ BR (pH 5.0). (B) SW voltammograms for cadmium oxidation performed at CB/G/PLA (black line) and CB/Ag-G/PLA (blue line) in the linear range of 4.5–100 µg L$^{-1}$ and 1.5–100 µg L$^{-1}$ in 0.1 mol L$^{-1}$ BR, respectively. Inset: calibration plots for CB/Ag-G/PLA. SWV parameters: $a = 80$ mV, $f = 40$ Hz, $\Delta E = 6$ mV, $E_{\text{deposition}} = -1.1$ V.
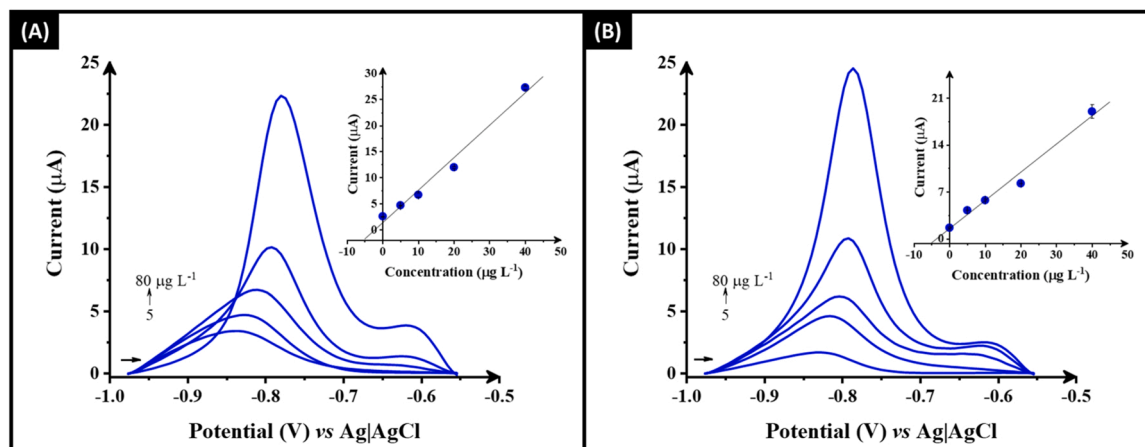
**Fig. 4.** SW voltammograms for cadmium oxidation in (A) diluted tap water (5-fold) and (B) in diluted river water (20-fold) in 0.1 mol L$^{-1}$ BR (pH 5.0) performed with AgNP-graphite in a concentration range of 5–80 µg L$^{-1}$. Inset: calibration curve obtained by the standard addition method. SWV parameters: $a$ = 80 mV, $f$ = 40 Hz, $\Delta E$ = 6 mV, $E_{deposition}$ = −1.1 V, and $t_{deposition}$ = 60 s.

**Table 1**
Determination of cadmium (II) within spiked river water sample (n = 3) using the optimised SWV methodology.

| Electrode | Cd$^{2+}$ Added (µg L$^{-1}$) | Cd$^{2+}$ Found (µg L$^{-1}$) | Recovery (%) |
|---|---|---|---|
| CB/Ag-G/ | 5 | 5.1 ± 0.5 | 102.0 |
| PLA | 10 | 9.6 ± 0.3 | 96.0 |

tested in additive manufacturing and to develop enhanced filaments to increasingly open the scope of applications of this technology in water pollution monitoring field.

## CRediT authorship contribution statement

**Karen K.L. Augusto:** Writing – review & editing, Writing – original draft, Validation, Software, Methodology, Investigation, Formal analysis, Data curation, Conceptualization. **Elena Bernalte:** Writing – review & editing, Writing – original draft, Supervision, Project administration, Methodology, Investigation, Formal analysis, Data curation, Conceptualization. **Robert D. Crapnell:** Writing – review & editing, Writing – original draft, Conceptualization. **Hayley G. Andrews:** Formal analysis. **Orlando Fatibello-Filho:** Writing – review & editing, Writing – original draft, Supervision, Funding acquisition, Formal analysis. **Craig E. Banks:** Writing – review & editing, Writing – original draft, Visualization, Validation, Supervision, Software, Resources, Project administration, Methodology, Investigation, Funding acquisition, Formal analysis, Data curation, Conceptualization.

## Declaration of Competing Interest

The authors declare that they have no known competing financial interests or personal relationships that could have appeared to influence the work reported in this paper.

## Acknowledgements

## Appendix A. Supporting information

Supplementary data associated with this article can be found in the online version at doi:10.1016/j.jece.2025.116446.

## Data availability

Data will be made available on request.

## References

[1] J.F. García-Reyes, P. Ortega-Barrales, A. Molina-Díaz, Sensing of trace amounts of cadmium in drinking water using a single fluorescence-based optosensor, Microchem. J. 82 (2006) 94–99.

[2] A.G.-M. Ferrari, P. Carrington, S.J. Rowley-Neale, C.E. Banks, Recent advances in portable heavy metal electrochemical sensing platforms, Environ. Sci.: Water Res. Technol. 6 (2020) 2676–2690.

[3] Y. Yi, Y. Zhao, Z. Zhang, Y. Wu, G. Zhu, Recent developments in electrochemical detection of cadmium, Trends Environ. Anal. Chem. 33 (2022) e00152.

[4] W.H. Organization, Guidel. Drink. -Water Qual., 4th Ed., Inc. 1st Add. (2017).

[5] Y. Lai, L. Dong, X. Sheng, J. Chao, S. Yu, J. Liu, Monitoring the Cd2+ release from Cd-containing quantum dots in simulated body fluids by size exclusion chromatography coupled with ICP-MS, Anal. Bioanal. Chem. 414 (2022) 5529–5536.

[6] S. Özdemir, V. Okumuş, E. Kılınç, H. Bilgetekin, A. Dündar, B. Ziyadanoğulları, Pleurotus eryngii immobilized Amberlite XAD-16 as a solid-phase biosorbent for preconcentrations of Cd2+ and Co2+ and their determination by ICP-OES, Talanta 99 (2012) 502–506.

[7] M. Soylak, A. Kars, I. Narin, Coprecipitation of Ni2+ , Cd2+ and Pb2+ for preconcentration in environmental samples prior to flame atomic absorption spectrometric determinations, J. Hazard. Mater. 159 (2008) 435–439.

[8] Y. Huang, W. Chen, M. Dong, N. Li, L. Chen, L. Ling, et al., A novel fluorescence probe for the recognition of Cd2+ and its application, Spectrochim. Acta Part A: Mol. Biomol. Spectrosc. 301 (2023) 122979.

[9] E. Bernalte, S. Arévalo, J. Pérez-Taborda, J. Wenk, P. Estrela, A. Avila, et al., Rapid and on-site simultaneous electrochemical detection of copper, lead and mercury in the Amazon river, Sens. Actuators B: Chem. 307 (2020) 127620.

[10] A.G.-M. Ferrari, S.J. Rowley-Neale, C.E. Banks, Screen-printed electrodes: transitioning the laboratory in-to-the field, Talanta Open 3 (2021) 100032.

[11] M.J. Whittingham, R.D. Crapnell, C.E. Banks, Additively manufactured rotating disk electrodes and experimental setup, Anal. Chem. 94 (2022) 13540–13548.

[12] M.J. Whittingham, R.D. Crapnell, E.J. Rothwell, N.J. Hurst, C.E. Banks, Additive manufacturing for electrochemical labs: an overview and tutorial note on the production of cells, electrodes and accessories, Talanta Open 4 (2021) 100051.

[13] A. Abdalla, B.A. Patel, 3D printed electrochemical sensors, Annu. Rev. Anal. Chem. 14 (2021) 47–63.

[14] M. Attaran, The rise of 3-D printing: the advantages of additive manufacturing over traditional manufacturing, Bus. Horiz. 60 (2017) 677–688.

[15] C. Kalinke, N.V. Neumsteir, G. de Oliveira Aparecido, T.V. de Barros Ferraz, P.L. Dos Santos, B.C. Janegitz, et al., Comparison of activation processes for 3D printed PLA-graphene electrodes: electrochemical properties and application for sensing of dopamine, Analyst 145 (2020) 1207–1218.

[16] D.P. Rocha, R.G. Rocha, S.V. Castro, M.A. Trindade, R.A. Munoz, E.M. Richter, et al., Posttreatment of 3D-printed surfaces for electrochemical applications: A critical review on proposed protocols, Electrochem. Sci. Adv. 2 (2022) e2100136.

[17] R.S. Shergill, B.A. Patel, Preprinting saponification of carbon thermoplastic filaments provides ready-to-use electrochemical sensors, ACS Appl. Electron. Mater. 5 (2023) 5120–5128.

[18] R.S. Shergill, F. Perez, A. Abdalla, B.A. Patel, Comparing electrochemical pre-treated 3D printed native and mechanically polished electrode surfaces for analytical sensing, J. Electroanal. Chem. 905 (2022) 115994.

[19] E. Bernalte, R.D. Crapnell, O.M. Messai, C.E. Banks, The effect of slicer infill pattern on the electrochemical performance of additively manufactured electrodes, ChemElectroChem (2024) e202300576.

[20] R.D. Crapnell, A. Garcia-Miranda Ferrari, M.J. Whittingham, E. Sigley, N.J. Hurst, E.M. Keefe, et al., Adjusting the connection length of additively manufactured electrodes changes the electrochemical and electroanalytical performance, Sensors 22 (2022) 9521.

[21] R. Shergill, B. Patel, 2022, The effects of material extrusion printing speed on the conductivity of carbon black/polylactic acid electrodes, (2022)..

[22] R.S. Shergill, C.L. Miller, B.A. Patel, Influence of instrument parameters on the electrochemical activity of 3D printed carbon thermoplastic electrodes, Sci. Rep. 13 (2023) 339.

[23] R.S. Shergill, B.A. Patel, The effects of material extrusion printing speed on the electrochemical activity of carbon black/polylactic acid electrodes, ChemElectroChem 9 (2022) e202200831.

[24] R.M. Cardoso, C. Kalinke, R.G. Rocha, P.L. Dos Santos, D.P. Rocha, P.R. Oliveira, et al., Additive-manufactured (3D-printed) electrochemical sensors: a critical review, Anal. Chim. Acta 1118 (2020) 73–91.

[25] R.D. Crapnell, E. Bernalte, A.G.-M. Ferrari, M.J. Whittingham, R.J. Williams, N. J. Hurst, et al., All-in-one single-print additively manufactured electroanalytical sensing platforms, ACS Meas. Sci. Au 2 (2021) 167–176.

[26] A.G.-M. Ferrari, N.J. Hurst, E. Bernalte, R.D. Crapnell, M.J. Whittingham, D. A. Brownson, et al., Exploration of defined 2-dimensional working electrode shapes through additive manufacturing, Analyst 147 (2022) 5121–5129.

[27] D.P. Rocha, A.L. Squissato, S.M. da Silva, E.M. Richter, R.A.A. Munoz, Improved electrochemical detection of metals in biological samples using 3D-printed electrode: Chemical/electrochemical treatment exposes carbon-black conductive sites, Electrochim. Acta 335 (2020) 135688.

[28] M. Choinska, V. Hrdlička, I. Šestáková, T. Navrátil, Voltammetric determination of heavy metals in honey bee venom using hanging mercury drop electrode and PLA/carbon conductive filament for 3D printer, Mon. F. üR. Chem. - Chem. Mon. 152 (2021) 35–41.

[29] R.D. Crapnell, C. Kalinke, L.R.G. Silva, J.S. Stefano, R.J. Williams, R.A.A. Munoz, et al., Additive manufacturing electrochemistry: an overview of producing bespoke conductive additive manufacturing filaments, Mater. Today 71 (2023) 73–90.

[30] P. Wuamprakhon, R.D. Crapnell, E. Sigley, N.J. Hurst, R.J. Williams, M. Sawangphruk, et al., Recycled additive manufacturing feedstocks for fabricating high voltage, low-cost aqueous supercapacitors, Adv. Sustain. Syst. 7 (2023) 2200407.

[31] E. Sigley, C. Kalinke, R.D. Crapnell, M.J. Whittingham, R.J. Williams, E.M. Keefe, et al., Circular economy electrochemistry: creating additive manufacturing feedstocks for caffeine detection from post-industrial coffee pod waste, ACS Sustain. Chem. Eng. 11 (2023) 2978–2988.

[32] R.D. Crapnell, I.V. Arantes, J.R. Camargo, E. Bernalte, M.J. Whittingham, B. C. Janegitz, et al., Multi-walled carbon nanotubes/carbon black/rPLA for high-performance conductive additive manufacturing filament and the simultaneous detection of acetaminophen and phenylephrine, Microchim. Acta 191 (2024) 96.

[33] C. Kalinke, R.D. Crapnell, E. Sigley, M.J. Whittingham, P.R. de Oliveira, L. C. Brazaca, et al., Recycled additive manufacturing feedstocks with carboxylated multi-walled carbon nanotubes toward the detection of yellow fever virus cDNA, Chem. Eng. J. 467 (2023) 143513.

[34] I.V. Arantes, R.D. Crapnell, E. Bernalte, M.J. Whittingham, T.R. Paixão, C.E. Banks, Mixed graphite/carbon black recycled PLA conductive additive manufacturing filament for the electrochemical detection of oxalate, Anal. Chem. 95 (2023) 15086–15093.

[35] K.K. Augusto, R.D. Crapnell, E. Bernalte, S. Zighed, A. Ehamparanathan, J. L. Pimlott, et al., Optimised graphite/carbon black loading of recycled PLA for the production of low-cost conductive filament and its application to the detection of β-estradiol in environmental samples, Microchim. Acta 191 (2024) 375.

[36] J.R. Camargo, R.D. Crapnell, E. Bernalte, A.J. Cunliffe, J. Redfern, B.C. Janegitz, et al., Conductive recycled PETg additive manufacturing filament for sterilisable electroanalytical healthcare sensors, Appl. Mater. Today 39 (2024) 102285.

[37] R.D. Crapnell, E. Bernalte, E. Sigley, C.E. Banks, Recycled PETg embedded with graphene, multi-walled carbon nanotubes and carbon black for high-performance conductive additive manufacturing feedstock, RSC Adv. 14 (2024) 8108–8115.

[38] I.V. Arantes, R.D. Crapnell, M.J. Whittingham, E. Sigley, T.R. Paixão, C.E. Banks, Additive manufacturing of a portable electrochemical sensor with a recycled conductive filament for the detection of atropine in spiked drink samples, ACS Appl. Eng. Mater. 1 (2023) 2397–2406.

[39] R.D. Crapnell, I.V. Arantes, M.J. Whittingham, E. Sigley, C. Kalinke, B.C. Janegitz, et al., Utilising bio-based plasticiser castor oil and recycled PLA for the production of conductive additive manufacturing feedstock and detection of bisphenol A, Green. Chem. (2023).

[40] E. Koukouviti, A. Economou, C. Kokkinos, 3D printable multifunctional electrochemical nano-doped biofilament, Adv. Funct. Mater. (2024) 2402094.

[41] A. Abbas, H.M.A. Amin, Silver nanoparticles modified electrodes for electroanalysis: An updated review and a perspective, Microchem. J. 175 (2022) 107166.

[42] J.P. Hughes, P.L. dos Santos, M.P. Down, C.W. Foster, J.A. Bonacin, E.M. Keefe, et al., Single step additive manufacturing (3D printing) of electrocatalytic anodes and cathodes for efficient water splitting, Sustain. Energy Fuels 4 (2020) 302–311.

[43] K. Partanen, Y. Pei, P. Hillen, M. Hassan, K. McEleney, G. Schatte, et al., Investigating electrochemical deposition of gold on commercial off-the-shelf 3-D printing materials towards developing sensing applications, RSC Adv. 12 (2022) 33440–33448.

[44] R.K. Pandey, L. Chen, S. Teraji, H. Nakanishi, S. Soh, Eco-friendly, direct deposition of metal nanoparticles on graphite for electrochemical energy conversion and storage, ACS Appl. Mater. Interfaces 11 (2019) 36525–36534.

[45] E. Bernalte, K.K.L. Augusto, R.D. Crapnell, H.G. Andrews, O. Fatibello-Filho, C. E. Banks, Eco-friendly integration of gold nanoparticles into additive manufacturing filaments: advancing conductivity and electrochemical performance, RSC Appl. Interfaces (2025) 439–450.

[46] G. Greczynski, L. Hultman, The same chemical state of carbon gives rise to two peaks in X-ray photoelectron spectroscopy, Sci. Rep. 11 (2021) 1–5.

[47] E.M. Richter, D.P. Rocha, R.M. Cardoso, E.M. Keefe, C.W. Foster, R.A. Munoz, et al., Complete additively manufactured (3D-printed) electrochemical sensing platform, Anal. Chem. 91 (2019) 12844–12851.

[48] Y. Meng, A sustainable approach to fabricating Ag nanoparticles/PVA hybrid nanofiber and its catalytic activity, Nanomaterials 5 (2015) 1124–1135.

[49] D. Garibo, H.A. Borbón-Nuñez, J.N.D. de León, E. García Mendoza, I. Estrada, Y. Toledano-Magaña, et al., Green synthesis of silver nanoparticles using Lysiloma acapulcensis exhibit high-antimicrobial activity, Sci. Rep. 10 (2020) 12805.

[50] I.S. Lopes, B.N. Oliveira de Moraes, S. de Souza Barreto, L.Le Joncour, C. Couteau, M.R. Franzolin, et al., Green synthesis of antimicrobial silver–copper nanoparticles using Banana and pineapple peel extracts: a sustainable approach for biomaterial sterilization, Mater. Chem. Phys. 333 (2025) 130364.

[51] J.S. Afolayan, A.M. Varney, J.C. Thomas, S. McLean, C.C. Perry, A rapid microwave approach for 'one-pot' synthesis of antibiotic conjugated silver nanoparticles with antimicrobial activity against multi-drug resistant bacterial pathogens, Colloids Surf. B: Biointerfaces 245 (2025) 114280.

[52] J.I. Langford, A.J.C. Wilson, Scherrer after sixty years: a survey and some new results in the determination of crystallite size, J. Appl. Crystallogr. 11 (1978) 102–113.

[53] A.K. Bishoyi, C.R. Sahoo, P. Samal, N.P. Mishra, B.R. Jali, M.S. Khan, et al., Unveiling the antibacterial and antifungal potential of biosynthesized silver nanoparticles from Chromolaena odorata leaves, Sci. Rep. 14 (2024) 7513.

[54] A.K. Thompson, C. Hackett, T.L. Grady, S. Enyinnia, Q.C. Moore, F.M. Nave, Development and characterization of membranes with PVA containing silver particles: a study of the addition and stability, Polymers 12 (2020) 1937.

[55] R.D. Crapnell, C.E. Banks, Perspective: what constitutes a quality paper in electroanalysis? Talanta Open 4 (2021) 100065.

[56] R.G. Compton, C.E. Banks, Understanding voltammetry, World Scientific, 2018.